Research Article Vol. 5, No. 4 / April 2018 / Optica 402

Direct sampling of a light wave in air

Seung Beom Park,[1] Kyungseung Kim,[1] Wosik Cho,[1,2] Sung In Hwang,[1] Igor Ivanov,[1] Chang Hee Nam,[1,2] and Kyung Taec Kim[1,2,*]

[1]Center for Relativistic Laser Science, Institute for Basic Science, Gwangju 61005, South Korea
[2]Department of Physics and Photon Science, Gwangju Institute of Science and Technology, Gwangju 61005, South Korea
*Corresponding author: kyungtaec@gist.ac.kr

Received 1 November 2017; revised 26 February 2018; accepted 8 March 2018 (Doc. ID 312589); published 2 April 2018

Temporal characterization of a laser pulse is an essential task in many applications. Temporal characterization methods that are currently available support only a limited spectral bandwidth without information on the carrier-envelope phase (CEP) of the laser pulse or require complicated equipment in a vacuum environment. Here we demonstrate that an arbitrary time-dependent laser field can be directly sampled using subcycle tunneling ionization in a gaseous medium or in air. The subcycle ionization is used as a fast temporal gate for the direct sampling of the laser field. This unique approach enables the complete temporal characterization of the laser field, including its CEP, for a broad spectral range in ambient air, providing a universal tool for the precise measurement of the laser field.

OCIS codes: (320.0320) Ultrafast optics; (250.0250) Optoelectronics; (260.3230) Ionization.

https://doi.org/10.1364/OPTICA.5.000402

1. INTRODUCTION

Rigorous temporal characterization of a laser pulse is essential for the precise description of light–matter interactions in many applications. Several techniques, using a nonlinear crystal, have been developed [1–3]. However, they suffer from the phase-matching issue of the nonlinear crystal, limiting the applicable wavelength range, and are not sensitive to the carrier-envelope phase (CEP) of a laser field. A complete temporal characterization of an arbitrary laser field could not be achieved with conventional approaches.

An arbitrary laser field can be sampled when a suitable subcycle temporal gate is available. Either attosecond x-ray pulses [4–6] emitted through high harmonic generation (HHG) or subcycle electron trajectories [7,8] in the HHG process can be used to measure a light wave [9]. Both techniques enable complete measurement of a time-dependent light wave, including CEP and higher-order dispersion for a broad spectral range [10,11]. However, they both require attosecond x-ray pulse generation and detection equipment in vacuum. They cannot easily be utilized in practical applications in which the direct conversion of a light wave into electric current is ideal [12–15]. Consequently, a radically different approach is needed for the direct sampling of a light wave.

Here, we demonstrate the direct sampling of a light wave using tunneling ionization in a gaseous medium or in air. In our approach, called the tunneling ionization with a perturbation for the time-domain observation of an electric field (TIPTOE) method, the tunneling ionization is used to sample a light wave. A signal pulse to be measured is superposed on an intense laser pulse. The signal pulse gently perturbs the process of the tunneling ionization, leading to the modulation of the total ionization yield that can be measured directly as an electric current. Our approach can be applied for a broad spectral range for the UV, visible, or longer wavelength ranges without a vacuum environment. Thus, it can be used as a versatile tool for the field measurement of a light wave. Also, it opens the way to measuring and controlling electric current using a light wave with an attosecond temporal resolution, which will become a key element in future technology.

2. RESULTS

A. Subcycle Tunneling Ionization as a Temporal Gate

Tunneling ionization is a purely quantum mechanical phenomenon in which the electron dynamics is described by a probability wave function $|\Psi|^2$, as depicted in Fig. 1(a). When an atom is exposed to a strong laser field, the atomic potential (V_C) is deformed. A part of the wave function can tunnel through the Coulomb barrier, creating subcycle electron wave packets in each half optical cycle of the laser pulse. In our technique, the subcycle electron wave packet generated by the strong laser field, which we call the fundamental pulse E_F, is thus used as the fast temporal gate to probe a signal pulse E_S. The signal pulse is too weak to induce tunneling ionization (only ~0.1% or ~0.01% of the fundamental intensity), but it can perturb the tunneling ionization process when superposed with the fundamental pulse, changing the total ionization yield.

To describe the subcycle tunneling ionization of an atom in a strong laser field, it is convenient to introduce the concept of an instantaneous ionization rate $w(E)$. There are a few ionization models that have been successfully used to describe strong field

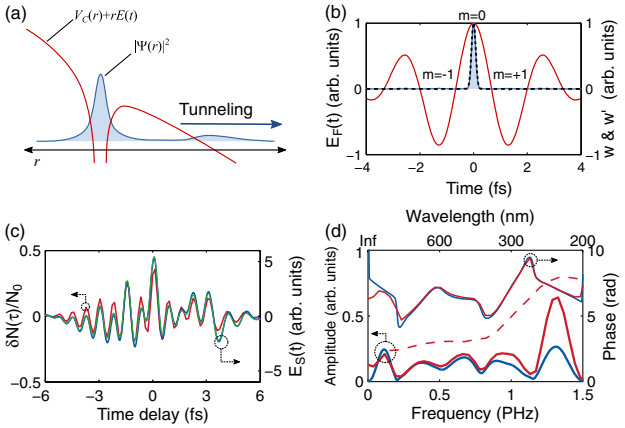

Fig. 1. (a) Tunneling ionization is illustrated. The part of the wavefunction (blue line) tunnels through the deformed potential barrier (red line). (b) The instantaneous ionization rate $w(t)$ (blue line) and its derivative with respect to the field strength $w'(t) = dw/dE|_{E=E_F(t)}$ (dotted line) calculated using the ADK ionization model for a He atom are shown. The fundamental laser pulse (center wavelength: 800 nm, duration: 3.9 fs in the FWHM, peak intensity: 1×10^{14} W/cm^2) used in the calculations is shown with the red line. (c) The numeral calculations were performed using the TDSE model in 3D. The fundamental pulse shown in (b) and the broadband signal pulse (blue line) were used in the calculation. The modulation of the ionization yield $\delta N/N_0$ obtained by solving the TDSE calculations is shown (red line). The modulation amplitude of the ionization yield for the same signal intensity is different for different wavelengths, as shown with the dashed line in (d). The modulation, after calibrating the spectral response (see Section S1.3 of Supplement 1), is shown as the green line. (d) The spectral amplitude (thick lines) and phase (thin lines) of the original (blue) and the calculated (red) pulses from the modulation of the ionization yield are shown. The spectral response of the TIPTOE measurement is shown with the dashed line (see Section S1.3 of Supplement 1).

phenomena, such as above-threshold ionization (ATI) and HHG in the tunneling regime [16–19]. In these models, the instantaneous ionization rate depends only on the field strength of the laser pulse. The superposition of the weak signal pulse can be approximated to the first order as $w(E_F + E_S) = w(E_F) + [dw(E)/dE|_{E=E_F}]E_S$ (see Section S1.1 of Supplement 1). Neglecting the depletion of the ground state, the total ionization yield N obtained by applying the two laser pulses can be written as $N = N_0 + \delta N$. Here, $N_0 = \int w(E_F)\mathrm{d}t$ is the ionization yield obtained by the fundamental pulse, and $\delta N = \int [dw(E)/dE|_{E=E_F}]E_S\,\mathrm{d}t$ is the modulation of the ionization yield due to the addition of the signal pulse. A universal feature of tunneling ionization is the exponential dependence of the ionization rate on intensity. Both the instantaneous ionization rate $w(E_F)$ and its derivative with respect to the field strength $dw(E)/dE|_{E=E_F}$ behave like a series of delta functions at every half optical cycle of the fundamental laser pulse due to the exponential dependence on the field strength, as illustrated in Fig. 1(b). The derivative $dw(E)/dE|_{E=E_F}$ provides a fast temporal gate at the peak of the pulse with a duration of about 190 attoseconds for the case shown in Fig. 1(b) in which the ionization rate and its derivative calculated using the Ammosov, Delong, and Krainov (ADK) ionization model [16] are shown. Assuming that the fundamental field has the cosine waveform (i.e., zero CEP), the modulation of the total ionization yield can be approximated as the sum of contributions from all half cycles,

$$\delta N(\tau) \propto \sum_{m=\ldots,-1,0,1,\ldots} a_m E_S\left(\tau + \frac{mT_F}{2}\right). \quad (1)$$

Here, a_m is a constant that represents the amplitude of the derivative $dw(E)/dE$ at the mth half optical cycle and T_F is the period of the fundamental pulse. If the fundamental pulse is so short that the ionization event effectively occurs only at the peak ($m = 0$), Eq. (1) can be simplified for an arbitrary signal pulse as

$$\delta N(\tau) \propto E_S(\tau). \quad (2)$$

The modulation of the ionization yield is proportional to the field amplitude of the signal pulse. This condition is satisfied when the fundamental pulse is shorter than around 1.5 optical cycles. The derivative $dw(E)/dE$ for $m = +1$ and $m = -1$ is only 1% of the peak at $m = 0$. Then, Eq. (2) is valid for a broad spectral range of the signal pulse if the excitation due to the signal pulse does not occur. For the atomic targets (He and H), the excitation does not occur up to 1.5 PHz (see Section S1.3 of Supplement 1). Consequently, the TIPTOE method can be applied for the broad spectral range of the signal pulse.

The validity of the TIPTOE method was examined using numerical calculations. The ionization yield was calculated in a He atom by solving a time-dependent Schrödinger equation (TDSE) in 3D [20]. The 3.9 fs (1.5 optical cycle) fundamental pulse was used at the intensity of 1×10^{14} W/cm^2. The signal pulse has a bandwidth of 1.3 PHz (from 220 nm to 3.7 μm in wavelength) in the FWHM, as shown in Figs. 1(c) and 1(d). The duration of the intensity envelope for the signal pulse shown in Fig. 1(c) is 590 as (1 as $= 10^{-18}$ s), and the duration of the electric field square is 280 as in FWHM. Even for this extreme case, the modulation of the ionization yield accurately reproduced the original signal pulse, as shown with the red line in Fig. 1(c). When the spectral response of the method shown in Fig. 1(d) is calibrated, the accuracy of the reconstruction is improved, as shown with the green line in Fig. 1(c) (see also Section S1.3 of Supplement 1 for the spectral response of the TIPTOE measurement). Note that the spectral calibration is not necessary when the fundamental and signal pulses have the similar bandwidth. Thus, it is not applied for the experimental data shown in Figs. 4–6. These numerical calculations support the validity of the TIPTOE measurement for the arbitrary PHz light wave.

In Eq. (2), neither the atomic excitation before tunneling nor the electron–ion interactions after tunneling are taken into account. The addition of the signal pulse can alter the electron trajectory after tunneling, thereby affecting the electron–ion interactions, known as the rescattering process [21]. Our numerical calculations that include these effects confirm that the excitation and electron–ion interactions do not affect the accuracy of Eq. (2), as shown in Figs. 1(c) and 1(d). Since we used the single active electron approximation in the calculations, multielectron effects such as double ionization were not included. However, their combined contribution to the total ionization yield is less than 1% [22,23]. Since the double ionization cross section is a slowly varying function of the kinetic energy of the returning electron, and the signal beam does not much change the kinetic energy of the electrons, their contribution in the modulation should remain less than 1% [24]. Therefore, the multielectron effects should be insignificant in the TIPTOE measurement.

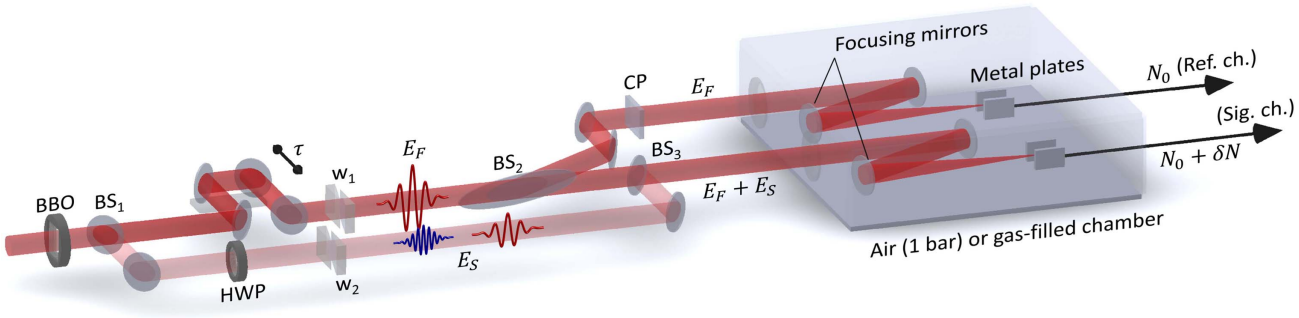

Fig. 2. Incident laser pulse is separated into two pulses: the fundamental pulse E_F and the signal pulse E_S. The fundamental pulse is divided into two identical pulses again by a beam splitter (BS2). One of these components is superposed with the signal pulse by another beam splitter (BS3). A part of the fundamental (730 nm, 5 fs pulses) or second-harmonic (355 nm) pulse can be selected as a signal pulse since the pulses are temporally separated. In the reference channel, the ionization yield N_0 is measured using only the fundamental pulse. In the signal channel, the ionization yield $N_0 + \delta N$ is measured using the fundamental and signal pulses. The details of the setup are provided in Section 4 (Methods).

The total ionization yield from tunneling ionization was measured using two metal plates connected to a signal amplifier and a data acquisition board in the experiment. The details of the experiment setup to perform the TIPTOE measurement, illustrated in Fig. 2, are explained in Section 4 (Methods). In the experiments, the ionization yield can also be modulated by the power fluctuation of the laser pulses. To compensate the modulation caused by the power fluctuation, the total ionization yield was differentially detected, as shown in Fig. 2. In the reference channel, the total ionization yield N_0 produced by the fundamental pulse only was measured. In the signal channel, the total ionization yield $N_0 + \delta N$ produced by both the fundamental and signal pulses was measured. The modulation of the total ionization yield due to the power fluctuation of the fundamental pulse could thus be canceled, and the modulation of the ionization yield was obtained with the ratio $\delta N/N_0$ as a function of the time delay. Consequently, the contribution of the signal pulse could be measured precisely. It should be noted that the differential detection is not essentially required for the TIPTOE measurement. The TIPTOE method can be applied without the reference channel. Since the power fluctuation of the laser causes a random noise, it can be removed by applying the spectral filtering or averaging the data (see Section S2 of Supplement 1).

B. Determination of the CEP of the Fundamental Pulse

The CEP of the fundamental pulse should be set to zero to measure the signal pulse accurately including the CEP. In this work, the second-harmonic signal pulse is used to find the CEP of the fundamental pulse, as described in Fig. 3, but other techniques can also be used [11,25]. For a cosine fundamental pulse (zero CEP), the contribution of the central peak to the total ionization yield is much greater than the contributions of the adjacent peaks, as shown in Fig. 3(a). The total ionization yield is modulated at the frequency of the second-harmonic signal pulse. On the other hand, in the case of a sine fundamental pulse, two dominant ionizations near the central peak (at $t = -T_0/4$ and $t = +T_0/4$, where T_0 is a period of the fundamental pulse) contribute to the total ionization yield. The superposed

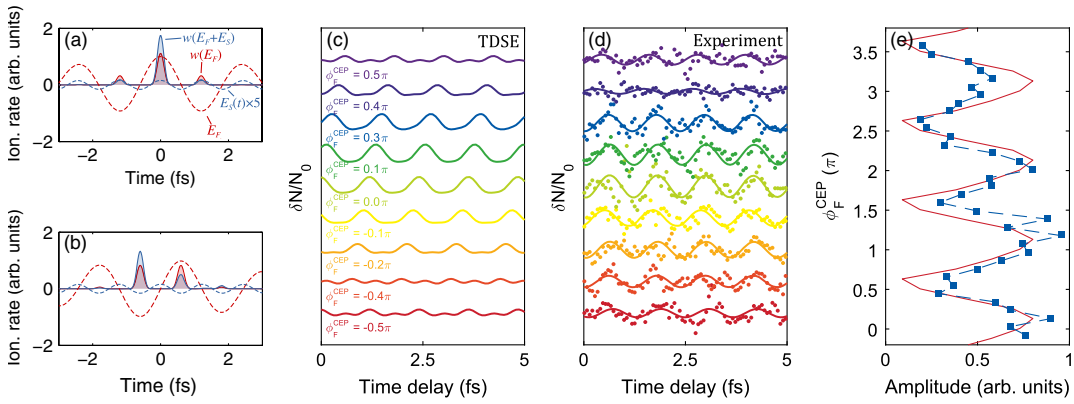

Fig. 3. (a), (b) ADK ionization rates calculated for Ar atoms using a 5 fs Gaussian (a) cosine or (b) sine pulse with an intensity of 1×10^{14} W/cm^2. The ionization rates obtained only with the fundamental field E_F are represented by solid red lines, while those obtained with the fundamental field E_F and the second-harmonic signal field E_S are shown with solid blue lines. In each case, the intensity of the second-harmonic field was 0.1% of the intensity of the fundamental field. (c) Results of *ab initio* calculations performed using the fundamental and second-harmonic signal pulses and different fundamental pulse CEPs ϕ_F^{CEP}. (d) Experimentally obtained total ionization yields corresponding to different CEPs. The ionization yields from Ar atoms (5 mbar) were obtained using the fundamental pulse (duration: 5 fs, center wavelength: 730 nm, peak intensity: 1×10^{14} W/cm^2) and the second-harmonic signal pulse (duration: ~100 fs, center wavelength: 355 nm). Nine cases corresponding to fundamental pulse CEPs ranging from 1.60π to 2.43π are represented by solid lines. The depicted ionization yields were obtained after narrow bandpass filtering (solid lines) and low-pass filtering (dots). (e) Comparison of the amplitude modulation results of the *ab initio* calculations (red line) and the experiments (blue boxes) for different CEPs.

second-harmonic signal increases the ionization yield for a half optical cycle, but it decreases the ionization yield for the next half optical cycle, as shown in Fig. 3(b). Thus, the contributions of the two dominant ionizations cancel each other out, and the modulation amplitude of the total ionization yield is much weaker than that obtained using the cosine fundamental pulse. The result of the TDSE calculations, presented in Fig. 3(c), further supports these interpretations. The differences between the amplitudes resulting from using different CEPs are also observable in the experimental results depicted in Fig. 3(d). Since the amplitude is maximized when the CEP of the fundamental pulse is set to zero, the CEP of the fundamental pulse at the focus where the TIPTOE measurement takes place can be determined, as shown in Fig. 3(e).

C. Validation of the TIPTOE Measurements

For a proof-of-concept of the TIPTOE method, a waveform measurement was carried out using few-cycle laser pulses. After setting the CEP of the fundamental laser pulse, a few-cycle laser pulse was used as a signal. The TIPTOE measurement was carried out for different CEPs; the results of these measurements are presented in Fig. 4. As the CEP of the signal pulse changes, the CEP of the signal pulse clearly evolves, as illustrated by the results in Fig. 4(a). Note that the shape of the envelope is not changed much when the CEP of the signal pulse varies from cosine to sine, as shown in Figs. 4(b) and 4(c). The duration of the signal pulse, measured while changing the CEP, was 4.8 ± 0.5 fs. The CEP evolution agrees with the values expected from the thickness change of the glass wedge used to control the CEP. Thus, the measurement results demonstrate the applicability of the TIPTOE method for characterizing light waves, including their CEPs.

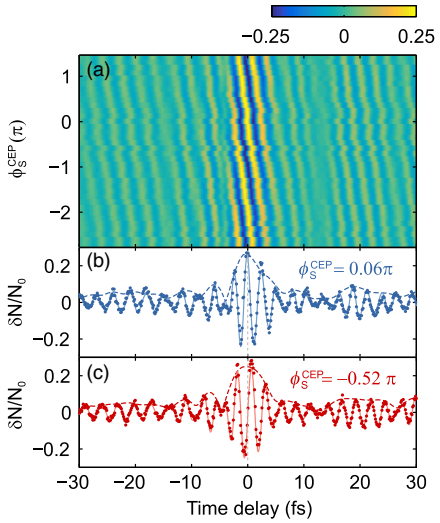

Fig. 4. Experiments were performed with few-cycle laser pulses. The intensity of the fundamental pulse was 1×10^{14} W/cm^2. The signal intensity was $\sim 1 \times 10^{11}$ W/cm^2. The modulation of the ionization yield was obtained in the Ar-filled chamber (5 mar). (a) Signal pulse measurements for different CEPs ϕ_S^{CEP} are shown. The color code shows the modulation of the ionization yield. (b), (c) The experimental data ($\delta N/N_0$) for cosine (b) and sine (c) signal pulses are shown (dots). The signal pulses (solid lines) and their envelopes (dashed lines) obtained after the spectral filtering from 500 nm to 1 μm are shown.

To confirm further the validity of the TIPTOE method, we compared the waveform measurements obtained using two different methods: the TIPTOE method and the petahertz optical oscilloscope method [7]. The waveforms of signal pulses were measured sequentially using both techniques (see Section S3 of Supplement 1). The two measurements show a very good agreement in all three cases: positively chirped [Fig. 5(a)], chirp-free [Fig. 5(b)], and negatively chirped [Fig. 5(c)] signal pulses. In Fig. 5(b), however, the amplitude of the chirp-free signal pulse measured using the petahertz optical oscilloscope is weaker than that obtained using the TIPTOE method. This discrepancy is due to the limited deflection angle of the harmonic radiation in the petahertz optical oscilloscope [26]. On the other hand, the TIPTOE results for the chirp-free case exhibit the correct amplitude increase, indicating the reliability of the TIPTOE method. The discrepancy can be corrected by using the spectral amplitude measured by the spectrometer (see Section S4 of Supplement 1).

Another validity check was performed by comparing the spectra acquired using different methods. The spectrum of each pulse was obtained by taking the Fourier transform of the experimentally measured waveform. As shown in Figs. 5(d)–5(f), the reconstructed spectra from the TIPTOE and the petahertz optical oscilloscope methods are almost identical to the spectrum measured using a grating-based optical spectrometer, confirming that the TIPTOE measurement yielded an accurate signal waveform. The spectral phases exhibit positive quadratic, flat, and negative quadratic phases for the positively chirped, chirp-free, and negatively chirped cases, respectively. The estimated group delay dispersions of the measurements ($+15.7$ fs^2, $+0.3$ fs^2, and -16.5 fs^2) agreed very well with the expected values ($+16.2$ fs^2, 0 fs^2, and -16.2 fs^2 for the positively chirped, chirp-free, and negatively chirped cases, respectively) that were determined from the thickness of the wedge insertion used for dispersion control. The spectral phase reconstruction results also show the periodic phase modulation imposed by the chirp mirrors, as indicated by the red arrows in Fig. 5(e). These measurements thus provided an additional proof of the validity and accuracy of the TIPTOE method.

D. TIPTOE Measurements in Air

The TIPTOE method should work under ambient conditions. The experiments shown in Figs. 4 and 5 were performed using the atomic targets, Ar (Fig. 4) or Xe (Fig. 5) with a pressure of 5 mbar, in a gas-filled chamber for the comparison with the TDSE calculations and the results obtained from the petahertz optical oscilloscope. To verify the TIPTOE operation in air, we first performed the waveform measurements for different dispersions by inserting a glass wedge in low-pressure argon (5 mbar). Then, we opened the chamber and repeated the measurements in air (1 bar), as shown in Fig. 6. There is a shift in the group delay dispersion (GDD) measurements due to the dispersion of additional air (47 cm air propagation in the chamber), as shown in Fig. 6(a). The difference of the GDD obtained from the experiment is 10.4 fs^2, while the theoretical difference estimated for 47 cm propagation of the laser pulse at 760 nm in air is 10.9 fs^2, showing an exceptional accuracy of the measurements. The temporal profiles for the chirp-free case are compared in Fig. 6(b) and their spectral amplitudes and phases are compared in Fig. 6(c). They show almost identical pulse shapes, confirming the applicability of the TIPTOE method in air.

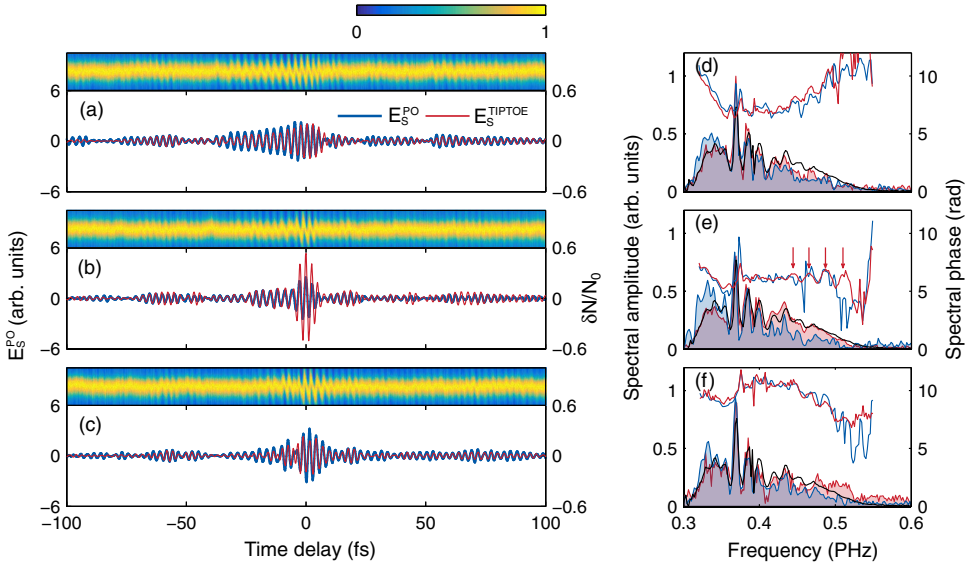

Fig. 5. (a)–(c) TIPTOE and petahertz optical oscilloscope (PO) measurements for signal pulses with different chirp conditions. In the TIPTOE measurements, the ionization yield from Xe atoms (5 mbar) was measured using the fundamental pulse (duration: 5 fs, center wavelength: 730 nm, intensity: 3×10^{13} W/cm^2). The dispersion of the signal pulse was controlled using a glass wedge to obtain (a) positively chirped, (b) chirp-free, and (c) negatively chirped pulses. The color plot at the top of each panel shows the spatial distribution of the harmonic radiation measured in the PO. In each case, the signal pulse was estimated based on the modulation of the spatial distribution. The signal electric fields measured using the PO method ESPO (τ) are shown with blue lines in (a)–(c), while those obtained using the TIPTOE method $\delta N/N_0$ are represented by red lines. The spectral filtering was applied to both the PO and TIPTOE results from 500 nm to 1 μm. (d)–(f) Spectral amplitudes (lower lines) and phases (upper lines) acquired using the PO (blue lines) and TIPTOE (red lines) methods for (d) positively chirped, (e) chirp-free, and (f) negatively chirped pulses. The spectral amplitudes measured with a grating-based optical spectrometer are shown with black lines for comparison in (d)–(f). The phase modulation caused by the chirp mirrors is marked with red arrows in (e).

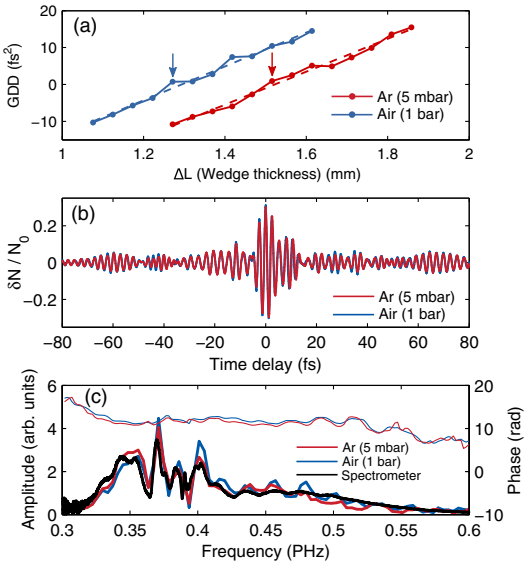

Fig. 6. (a) GDDs obtained for different glass thicknesses in air (blue) and in Ar (red) are shown. (b) The temporal profiles obtained at the chirp-free cases [marked with the arrows in (a)] for 1 bar air (blue) and 5 mbar Ar (red) are compared. (c) The spectral amplitudes for the pulses shown in (b) are shown for 1 bar air (thick blue) and 5 mbar Ar (thick red). The spectral amplitude measured with a spectrometer is shown (thick black). The spectral phases are shown for air (thin blue) and Ar (thin red). The spectral filtering is applied from 500 nm to 1 μm.

3. DISCUSSION

The TIPTOE method uses tunneling ionization as a fast temporal gate for the sampling of a laser field. This unique feature enables the complete temporal characterization of the laser field for many different situations. In this work, the validity of the method is confirmed using few-cycle laser pulses that cover the wavelength range from 500 nm to 1 μm. According to the numerical analysis shown in Fig. 1, the method can be employed across a broad spectral range covering a 1.5 PHz bandwidth for the wavelength longer than 200 nm without a vacuum requirement. As shown in Sections S1.2–1.3 of Supplement 1, the TIPTOE method can also be applied for multicycle laser pulses if the duration of the fundamental laser pulse is shorter than three times the transform-limited duration of the signal pulse. There is no restriction on the chirp condition of the signal pulse. The experimental verification for different wavelengths or long multicycle laser pulses, which is beyond the scope of this work, will be presented in future works.

In summary, we demonstrated a new pulse characterization method called TIPTOE in which an arbitrary laser field is directly sampled using tunneling ionization in a gaseous medium or in air. It is shown that the TIPTOE method can be used to measure the laser field including the CEP. The validity of the method is confirmed by comparing the results obtained with the petahertz optical oscilloscope using few-cycle laser pulses for different dispersion conditions. Since tunneling ionization universally occurs for a broad spectral range, the TIPTOE method will provide a versatile tool for the complete temporal characterization of a laser field.

4. METHODS

A 1 kHz CEP-stabilized Ti:sapphire laser was used in the experiment. The laser pulse was initially 25 fs long at the center wavelength of 800 nm. A few-cycle laser pulse was obtained by using a Ne-gas-filled (3.7 bar) 2 m long stretched hollow-core fiber with an inner diameter of 500 μm. The energy of the laser pulse used in the experiment was around 10 μJ. The energy jitter of the laser was around 1% rms at the place where the ionization is measured. After the second-harmonic beam was generated (BBO, 200 μm beta barium borate crystal), it was separated by a harmonic separator (BS1). The harmonic separator reflected both the fundamental (4%) and second-harmonic (>90%) components, which were temporally separated. Thus, a portion of the fundamental or the second harmonic could be used as the signal pulse, depending on the time delay.

The second-harmonic pulse was used as a signal pulse to determine the CEP of the fundamental pulse. Since the polarization direction of the signal pulse should be parallel to that of the fundamental pulse, the polarization of the second-harmonic pulse was rotated by a half-wave plate (HWP). The fundamental pulse, which had an incident angle of 80°, was divided into two identical pulses again by a fused silica glass beam splitter (BS2). The reflected fundamental pulse passed through a compensation plate (CP) to compensate for the dispersion in BS2. The fundamental pulse transmitted through BS2 was superposed with the signal pulse by another harmonic separator (BS3). Due to the reflectivity of the harmonic separator near 700 nm, the intensity of the signal pulse was reduced to ∼0.1% of the fundamental intensity after two reflections. The signal intensity was adjusted further by using a variable iris (not shown). The dispersion of each beam line was controlled by a pair of fused-silica wedges with an angle of 2.8° (W1, W2).

The ionization yield was differentially measured using the experiment setup shown in Fig. 2. In the signal channel, the fundamental pulse superposed with the signal pulse was focused between two parallel metal plates (each with dimensions of 1 cm × 1 cm) to obtain the ionization yield $N_0 + \delta N$. In the reference channel, the fundamental pulse without the signal pulse was focused between the other metal plates to obtain the reference ionization yield N_0. The electrons and ions were produced by the tunneling ionization between the biased metal plates. They can be accelerated and collide with other molecules, producing other electrons and ions. This post-ionization process is known as Townsend discharge, which can amplify the signal depending on the bias voltage and the gap (∼1 mm) between two metal plates. The metal plates were connected to current amplifiers (Keithley, 428 current amplifier), which applied bias voltages of 5 V and collected electrons and ions. When the measurement was carried out in air, the bias voltages of 200 V was applied by the separate power supplies (Stanford Research System, PS350). The peaks of the ionization signal for every pulse were recorded by the data acquisition boards (National Instrument, USB-6216) fast enough to capture the ionization yield at a 1 kHz or higher repetition rate with a 16 bit resolution. The time delay τ between the fundamental and signal pulses was controlled by a piezo stage (PI, P-629). The signal pulse precedes the fundamental pulse when the time delay is positive. The CEPs of the fundamental and signal pulses were independently controlled by wedge pairs W1 and W2. The polarization direction of the fundamental and signal pulses should be parallel. However, their directions with respect to the metal plates do not affect the measurement. The stability of the measurement was tested (see Section S2 of Supplement 1). It shows a 2.8% rms error in the duration measurement. After the TIPTOE measurements, we performed the petahertz optical oscilloscope measurement (see Section S3 of Supplement 1).

Funding. Institute for Basic Science (IBS-R012-D1).

See Supplement 1 for supporting content.

REFERENCES

1. D. J. Kane and R. Trebino, "Characterization of arbitrary femtosecond pulses using frequency-resolved optical gating," IEEE J. Quantum Electron. **29**, 571–579 (1993).
2. C. Iaconis and I. A. Walmsley, "Spectral phase interferometry for direct electric-field reconstruction of ultrashort optical pulses," Opt. Lett. **23**, 792–794 (1998).
3. M. Miranda, C. L. Arnold, T. Fordell, F. Silva, B. Alonso, R. Weigand, A. L'Huillier, and H. Crespo, "Characterization of broadband few-cycle laser pulses with the d-scan technique," Opt. Express **20**, 18732–18743 (2012).
4. M. Hentschel, R. Kienberger, C. Spielmann, G. A. Reider, N. Milosevic, T. Brabec, P. Corkum, U. Heinzmann, M. Drescher, and F. Krausz, "Attosecond metrology," Nature **414**, 509–513 (2001).
5. E. Goulielmakis, M. Uiberacker, R. Kienberger, A. Baltuska, V. Yakovlev, A. Scrinzi, T. Westerwalbesloh, U. Kleineberg, U. Heinzmann, M. Drescher, and F. Krausz, "Direct measurement of light waves," Science **305**, 1267–1269 (2004).
6. M. Garg, M. Zhan, T. T. Luu, H. Lakhotia, T. Klostermann, A. Guggenmos, and E. Goulielmakis, "Multi-petahertz electronic metrology," Nature **538**, 359–363 (2016).
7. K. T. Kim, C. Zhang, A. D. Shiner, B. E. Schmidt, F. Légaré, D. M. Villeneuve, and P. B. Corkum, "Petahertz optical oscilloscope," Nat. Photonics **7**, 958–962 (2013).
8. A. S. Wyatt, T. Witting, A. Schiavi, D. Fabris, P. Matia-Hernando, I. A. Walmsley, J. P. Marangos, and J. W. G. Tisch, "Attosecond sampling of arbitrary optical waveforms," Optica **3**, 303–310 (2016).
9. M. Chini, K. Zhao, and Z. Chang, "The generation, characterization and applications of broadband isolated attosecond pulses," Nat. Photonics **8**, 178–186 (2014).
10. A. Baltuška, T. Udem, M. Uiberacker, M. Hentschel, E. Goulielmakis, C. Gohle, R. Holzwarth, V. S. Yakovlev, A. Scrinzi, T. W. Hänsch, and F. Krausz, "Attosecond control of electronic processes by intense light fields," Nature **421**, 611–615 (2003).
11. G. G. Paulus, F. Grasbon, H. Walther, P. Villoresi, M. Nisoli, S. Stagira, E. Priori, and S. De Silvestri, "Absolute-phase phenomena in photoionization with few-cycle laser pulses," Nature **414**, 182–184 (2001).
12. M. Schultze, E. M. Bothschafter, A. Sommer, S. Holzner, W. Schweinberger, M. Fiess, M. Hofstetter, R. Kienberger, V. Apalkov, V. S. Yakovlev, M. I. Stockman, and F. Krausz, "Controlling dielectrics with the electric field of light," Nature **493**, 75–78 (2013).
13. A. Schiffrin, T. Paasch-Colberg, N. Karpowicz, V. Apalkov, D. Gerster, S. Mühlbrandt, M. Korbman, J. Reichert, M. Schultze, S. Holzner, J. V. Barth, R. Kienberger, R. Ernstorfer, V. S. Yakovlev, M. I. Stockman, and F. Krausz, "Optical-field-induced current in dielectrics," Nature **493**, 70–74 (2013).
14. E. Goulielmakis, V. S. Yakovlev, A. L. Cavalieri, M. Uiberacker, V. Pervak, A. Apolonski, R. Kienberger, U. Kleineberg, and F. Krausz, "Attosecond control and measurement: lightwave electronics," Science **317**, 769–775 (2007).
15. F. Krausz and M. I. Stockman, "Attosecond metrology: From electron capture to future signal processing," Nat. Photonics **8**, 205–213 (2014).
16. M. V. Ammosov, N. B. Delone, and V. P. Krainov, "Tunnel ionization of complex atoms and of atomic ions in an alternating electromagnetic field," Sov. Phys. JETP **64**, 1191–1194 (1986).
17. L. V. Keldysh, "Ionization in the field of a strong electromagnetic wave," Sov. Phys. JETP **20**, 1307 (1965).
18. A. M. Perelemov, V. S. Popov, and M. V. Terent'ev, "Ionization of atoms in an alternating electric field," Sov. Phys. JETP **23**, 924 (1966).

19. V. S. Popov, "Tunnel and multiphoton ionization of atoms and ions in a strong laser field (Keldysh theory)," Phys.-Usp. **47**, 855–885 (2004).
20. I. A. Ivanov, "Evolution of the transverse photoelectron-momentum distribution for atomic ionization driven by a laser pulse with varying ellipticity," Phys. Rev. A **90**, 013418 (2014).
21. P. B. Corkum, "Plasma perspective on strong field multiphoton ionization," Phys. Rev. Lett. **71**, 1994–1997 (1993).
22. A. L'Huillier, L. A. Lompre, G. Mainfray, and C. Manus, "Multiply charged ions formed by multiphoton absorption processes in the continuum," Phys. Rev. Lett. **48**, 1814–1817 (1982).
23. B. Walker, B. Sheehy, L. F. DiMauro, P. Agostini, K. J. Schafer, and K. C. Kulander, "Precision measurement of strong field double ionization of helium," Phys. Rev. Lett. **73**, 1227–1230 (1994).
24. Z. Chen, Y. Liang, D. H. Madison, and C. D. Lin, "Strong-field nonsequential double ionization of Ar and Ne," Phys. Rev. A **84**, 023414 (2011).
25. W. P. Putnam, R. G. Hobbs, P. D. Keathley, K. K. Berggren, and F. X. Kärtner, "Optical-field-controlled photoemission from plasmonic nanoparticles," Nat. Phys. **13**, 335–339 (2017).
26. K. T. Kim, K. Kim, and T. J. Hammond, "Phase retrieval approach for an accurate reconstruction of an arbitrary optical waveform in the petahertz optical oscilloscope," J. Phys. B **50**, 024002 (2017).